Transport in Porous Media (2020) 133:119–138
https://doi.org/10.1007/s11242-020-01417-w

The Mechanism for Improved Polymer Gel Blocking During Low-Salinity Waterfloods, Investigated Using Positron Emission Tomography Imaging

Bergit Brattekås[1] · **Randy Seright**[2]

Received: 28 August 2019 / Accepted: 25 April 2020 / Published online: 6 May 2020

Abstract

Polymer gels can be placed in fractures within subsurface reservoirs to improve sweep efficiency during subsequent floods, and its success is largely determined by the gel's ability to completely occupy the fracture volume. Gel volumetric properties may be influenced by mechanical and chemical conditions. In this work, gel volume sensitivity to salinity contrast is investigated. Previous bulk gel studies showed that water-based gel swelled in contact with lower-salinity water and shrunk in contact with higher-salinity water. Recent core-scale experiments demonstrated that gel blocking efficiency after rupture was also impacted by the salinity of the injected water phase. Gel treatments (after gel rupture) become less efficient in controlling fracture flow with time and water throughput during water injection without salinity contrasts. However, by reducing the salinity of the injected water phase with respect to the gel, blocking efficiency may be maintained, or even improved, over time. The coupling between gel deformation during swelling/shrinking and dynamic fluid flow is complex and can initiate changes in mechanical or transport properties, included formation of fluid flow paths through the gel that are not easily distinguished during conventional core floods. In-situ imaging by positron emission tomography (PET) was utilized to gain access to local flow patterns in this work, and combined with pressure measurements to characterize complex flow phenomena in a fractured, gel-filled system. Gel rupture was quantified several consecutive times during low-salinity waterflooding. Increasing rupture pressures indicates continuous gel strengthening during low-salinity water injection. PET imaging revealed that gel swelling occurred during low-salinity waterfloods, to constrict water pathways through the fracture. Gel swelling was sufficient to restrict fracture flow completely, and injected water was diverted into the rock matrix adjacent to the fracture. Injected water continued to pass through gel at elevated pressure gradients, but continuous flow paths did not form. This observation supports the notion of gel as a compressible, porous medium.

Keywords Polymer gel · Low-salinity waterflooding · Blocking mechanism · PET imaging

✉ Bergit Brattekås
bergit.brattekas@uib.no

[1] Department of Physics and Technology, University of Bergen, Bergen, Norway

[2] Petroleum Recovery Research Center (PRRC), New Mexico Institute of Mining and Technology, Socorro, USA

1 Introduction

Polymer gel is often injected into subsurface reservoirs to reduce fracture conductivity; hence, subsequently injected fluids may be diverted into the porous rock instead of channeling through the highly conductive fracture network (see, e.g., Sydansk and Romero-Zerôn 2011). Establishing matrix flow is important to access as much as possible of the pore volume during large-scale sequestering of CO_2 in subsurface sedimentary reservoirs, as well as during hydrocarbon recovery. Polymer gel may also be used to stimulate fractures in hydraulic fracturing applications (see, e.g., Ely and Herndon 2019).

Decades of research have described gel as inherently complex substances with combined liquid and solid behavior. Although polymer gels macroscopically may be perceived as fluids, the inner structure consists of interconnected polymer molecules holding a large quantity of solvent (mostly water). Thus, gel may be defined as flexible porous media, where the polymer structure of the gel constitutes a matrix of constant solid volume and the gel porosity is defined by the volume fraction of solvent (Andersen et al. 2019). The concentrations of polymer and crosslinker necessary to form gel are low: The gel system in this paper consists of 5000 ppm polymer, 417 ppm crosslinker and almost 99.5% water. Despite its high water content, high viscous gel forms within 5 h when the solution is subjected to an elevated temperature of 41 °C (~2.7×10^6 cP according to Liu and Seright 2001). Gel was injected into a fractured system in this paper. The polymer structure of fully formed gel is restricted to fractures during injection, but the water content of the gel may be reduced by leakoff, further described by Seright (2003a, b) and Brattekås et al. (2019). The driving force for leakoff is the pressure drop between the gel propagating through the fracture and the adjacent matrix. The remaining polymer gel structure becomes immobile when losing water and settles in the vicinity of where the dehydration occurred. Dehydrated gel nucleates locally within the fracture, eventually forming a non-uniform gel cake. At the end of gel injection, an uneven polymer concentration is expected within the fracture, i.e., most of the fracture volume is filled with dehydrated gel, with a range of concentrations. Gel of the injected concentration (i.e., gel that did not dehydrate) exists within the gel cake in designated channels termed *wormholes*. The presence of wormholes is important during subsequent fluid injections because the gel within the wormholes is more likely to be displaced than the adjacent, more concentrated gel cake. Wormholes were previously observed during gel injection Seright (2003a, b), by injecting dye, and after subsequent waterfloods by visual inspections of the fracture surfaces (Brattekås et al. 2015). Recently, in-situ imaging was also applied to visualize wormhole development during dynamic water injection, by applying magnetic resonance imaging (MRI) (Brattekås and Fernø 2016) or positron emission tomography imaging combined with computed tomography (PET-CT) (Brattekås et al. 2017; Brattekås and Seright 2018). Gel behavior during subsequent waterfloods without salinity contrasts was well-mapped using PET imaging (Brattekås et al. 2017). When the imposed pressure gradient reaches the gel rupture pressure, non-concentrated gel is displaced, and a wormhole flow pattern forms within the gel-filled fracture. After gel rupture, the injected water preferentially flows within wormholes through partially gel-filled fractures. The wormhole size increases with time and water throughput, and the gel blocking efficiency decreases as the wormhole expands due to decreased flow resistance. This corroborate reports from several other authors, concluding that gel becomes decreasingly efficient in reducing fracture flow with time and water throughput when a pressure gradient is imposed on the gel (Ganguly et al. 2002; Seright 2003a, b; Willhite and Pancake 2008; Brattekås et al. 2015).

Volumetric changes in fracture-filling gel largely determine the fracture blocking efficiency during subsequent fluid injections (Brattekås et al. 2016, 2017). Gel dehydration due to imposed pressure gradients (Al-Sharji et al. 1999; Krishnan et al. 2000; Wilton and Asghari 2007) is one example of negative volumetric changes (gel shrinkage) that may open parts of the gel-treated fracture to flow and significantly reduce the efficiency of the gel treatment. Gel shrinkage may also occur due to capillary pressure gradients (Brattekås et al. 2014), syneresis (Romero-Zeron et al. 2008) or interaction with reservoir fluids. Changes in external conditions around the gel volume, such as temperature, pH, ionic strength, external electric field or solvent composition, may also cause changes in the gel volume (Rydzewski 1990; Horkay et al. 2000). Water-based bulk gel generally shrinks if it is placed in water with a higher salinity than the gel solvent and swells when the salinity in the surrounding water phase is decreased (Rydzewski 1990; Bai et al. 2007; Aalaie et al. 2009; Tu and Wisup 2011; Zhang and Bai 2011). Rydzewski (1990) related the changes in volume to the change in osmotic pressure caused by the diffusion of sodium chloride to and from the solvent and the gel. Aalaie et al. (2009) pointed out that injected polymer gel may shrink in contact with cationic reservoir water. Tu and Wisup (2011) indicated that conformance could be improved by gel swelling in contact with lower-salinity formation brine. Brattekås et al. (2016) and Brattekås and Seright (2018) placed high-salinity gel in open fractures and injected lower-salinity water to determine if the salinity contrast could positively impact gel blocking. They found that the blocking efficiency of ruptured gel improved with time and water throughput during low-salinity water injections, contrary to standard water-chase floods. Gel swelling was proposed as the most likely cause for improved blocking, but "it remains unclear whether the gel swells uniformly to constrict wormholes, or if gel particles dislodge from the filter-cake, swell and clog in narrow parts of the wormhole" (Brattekås and Seright 2018). In this work, in-situ positron emission tomography imaging was applied to search for the mechanism behind improved gel blocking during low-salinity waterfloods. The gel was deliberately ruptured several times, by increasing the water injection rate. The rupture pressure was observed to increase, indicating that the dynamic injection of low-salinity water counteracted, or even reversed, mechanical gel degradation.

2 Materials and Methods

2.1 Preparations

A rectangular slab of outcrop Edwards limestone (from Garden City, West Texas) was used for this work. The core material had a heterogeneous, trimodal, pore size distribution yielding a range of porosity (15–30%) and permeability (3–40 mD) values (Tie 2006; Riskedal et al. 2008; Tipura 2008). A "fracture" was positioned longitudinally within the rectangular limestone core using a band saw, creating a smooth fracture with a constant fracture length (13 cm) and height (6.2 cm). The thickness of the matrix on each side of the fracture was 2.2 cm. The core surface was gently rinsed using tap water, and the core slab was thereafter dried at an elevated temperature of 60 °C. The core slab was assembled with an open fracture of 1-mm aperture by fixing specially made distribution POM (polyoxymethylene) end pieces to each end face. The end pieces facilitated a vertical spacer of 0.1-cm thickness, as shown in Fig. 1. Holes were drilled through the spacer to ensure an even distribution of injected fluids in the fracture. The inlet and outlet end faces were sealed, and the end

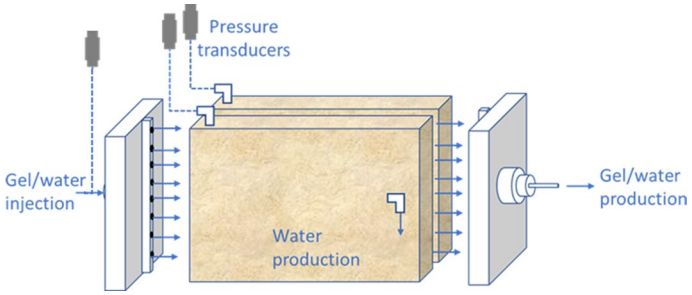

Fig. 1 Rectangular core with specially made distribution end pieces. The end pieces facilitated one common injection/production connection, which was branched into several small injection/production points evenly distributed within the fracture. The distribution points were drilled through a 1-mm spacer to facilitate direct injection of both gel and water into the fracture. Four Swagelok elbows were fitted in direct contact with the rock surface to facilitate measurements of matrix pressure and production

pieces were fixed to the end faces using epoxy resin. The core sides, top and bottom were also coated in several layers of epoxy resin to define no-flow boundaries. Four holes were drilled through the epoxy, two in each matrix, and fitted with Swagelok 1/8″ nylon elbows (Fig. 1). Pressure transducers were connected to the two matrix outlets located at the top of the core slab, 1 cm from the injection point, to measure the matrix pressure during injections. Two matrix outlets on the core circumference (1 cm from the fracture production outlet) facilitated production and quantification of matrix effluents. Hence, with the current setup, both gel and chase water were forcedly injected directly into the fracture, with only a few possible exit opportunities. The injected fluids could either pass through the fracture and be produced through the fracture outlet, or pass into the matrix to be produced through the matrix outlets.

The core was saturated by high-salinity water (4 wt% NaCl, 3.4 wt% $CaCl_2 \cdot 2H_2O$, 0.5 wt% $MgCl_2 \cdot 6H_2O$) under vacuum, and the porosity was determined by weight measurements to be 28%. Water of the same composition was injected into the fracture (with the fracture production outlet closed and the matrix production outlets open) to determine matrix conductivity. A pressure drop of approximately 15 psi was measured between the point of injection and matrix production outlets at an injection rate of 55 ml/h, with a linear dependency between varying flow rates and measured pressure; hence, the permeability of the slab was in the range of 0.2–200 mD, depending on the fracture surface area involved in flow. The absolute limitations, used for this calculation, were the total fracture surface area (maximum) and the elbow cross section (minimum). Previous publications suggest absolute permeability in the lower end of this range. Edwards limestone was also previously used in polymer gel studies (Brattekås et al. 2015; Brattekås and Seright 2018) and was chosen for this experiment due to the relatively low permeability of the core material. Post-processing of the PET signal is necessary to reconstruct PET images, i.e., matrix flow could not be visualized directly during the waterflood. Dynamic pressure measurements were, however, continuously available, and a notable pressure elevation was recorded when water entered the matrix. Gel-filled fractures through Edwards limestone were previously re-blocked in a timely manner during low-salinity waterflooding (Brattekås and Seright 2018), providing a reasonable time frame for imaging by PET.

Polymer gel was made by mixing commercially available HPAM polymer (5 million Daltons molecular weight) at 5000-ppm concentration in brine (same, high-salinity

composition) and adding 417 ppm of Cr(III)-acetate crosslinker to the polymer solution. The solution was thereafter aged at 41 °C for 24 h (five times the gelation time) to form polymer gel. Gel was injected into the fractured limestone core slab at ambient temperature and pressure conditions, using an injection rate of 200 cm^3/h for 4 h. Gel only passes through the fracture during injection and does not enter significantly into the matrix, due to its structure. The high water content in the gel was, however, reduced by leakoff during gel injection, driven by the pressure difference between the gel-filled fracture and adjacent matrix. The injection pressure gradient during gel injection was expected to increase swiftly and thereafter level out to a constant value, given by the equation $dP/dL = 0.02/w_f^2$ (Seright 2003a, b), where w_f is the fracture width. The measured injection pressure development (Fig. 2) exemplifies the expected behavior and also includes the recorded pressure drop in the matrix. Water leakoff was calculated by recording effluents produced from the matrix production outlets versus time. Brattekås et al. (2015) previously reported water leakoff rates for the same core material, using the same injection rate. The measured leakoff rate was lower in the current core (Fig. 2), presumably caused by the direct injection of gel into the fracture, preventing gel dehydration at the inlet end face. The main purpose of this study was to investigate low-salinity influence on wormhole development after gel rupture; hence, the leakoff rate was of less importance (although it was important that leakoff, in fact, occurred). Approximately, 100 fracture volumes (FV) were injected, during which the gel was continuously dehydrated by leakoff. At the end of gel injection, simple material balance calculations inferred that more than 95% of the longitudinal fracture volume was filled with concentrated, pressure-resistant gel.

2.2 PET-Imaging of Wormhole Development During Chase Water Injection

PET imaging is based on the decay of positron-emitting radionuclides and is routinely used as a diagnostic tool in medicine and pre-clinical research. PET was occasionally used to visualize fluids in porous structures, such as crystalline rocks (Degueldre et al. 1996), construction materials (Hoff et al. 1996) and sediments (Maguire et al. 1997; Khalili et al.

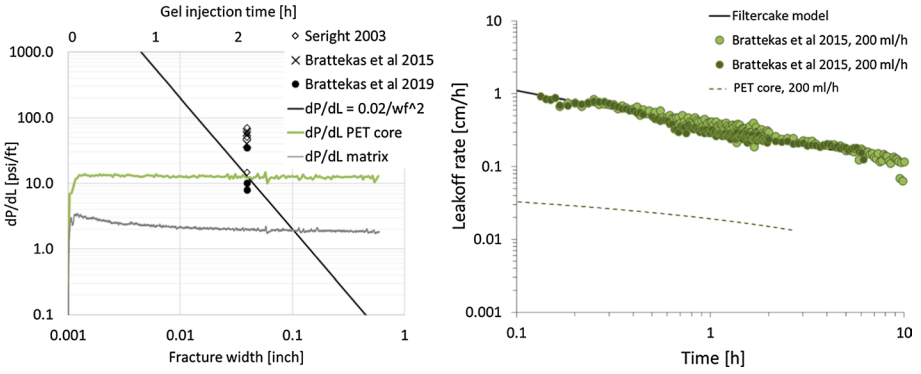

Fig. 2 Pressure gradient during gel injection (left) coincided with the equation $dP/dL = 0.02/w_f^2$ for a fracture width of 0.04 in. (1 mm) as proposed by Seright (2003a, b). The leakoff rate measured during gel injection into the limestone core slab (right) was lower than previously measured values, presumably caused by the closed inlet end face (leakoff only occurs inside the longitudinal fracture). The purpose of this study was to investigate dynamic wormhole development after gel rupture: Thus, the specific leakoff characteristics were of less importance, while it was of utmost importance that leakoff occurred

1998; Haugan 2000). Recent developments in PET imaging enabled core and sub-core-scale quantification of dynamic fluid flow in porous rocks (Kulenkampff' et al. 2008; Krevor et al. 2012; Fernø et al. 2015; Pini et al. 2016; Zahasky and Benson 2018). PET imaging is widely applicable in geoscience due to the availability of radiotracers, rendering explicit tracking of several fluid phases possible. An in-depth overview of PET imaging in water resources research may be found in Zahasky et al. (2019). PET imaging was previously demonstrated to be an efficient tool in distinguishing dynamic gel behavior during subsequent waterfloods (Brattekås et al. 2017, 2018). Wormhole development was visualized by radioactively labeling the injected brine by water-soluble ^{18}F-fluorodeoxyglucose (^{18}F-FDG), with a short half-life ($t_{1/2}$) of 109 min. Clearly, distinguishable wormholes were observed by PET during short time spans. However, radioactive decay caused difficulty in distinguishing wormholes during long-term injection of radioactively labeled low-salinity water (Brattekås and Seright 2018). In this work, two separate pumps were used and the experimental setup (Fig. 3) was designed to facilitate injection of radioactive water pulses. Radioactively labeled water was mixed into the injection stream at desired times and afterward displaced from the core using non-labelled water. ^{18}F was produced by a local cyclotron and used to synthesize ^{18}F-fluorodeoxyglucose (^{18}F-FDG), which was added to the injection water several times during the 50-h long waterflood.

The gel-filled, fractured limestone was placed in a high-resolution PET-CT scanner for imaging during subsequent waterflooding. PET images and dynamic pressure measurements were both used to determine gel behavior during long-term low-salinity waterflooding, by quantifying gel rupture, fracture-blocking efficiency and local flow patterns. Water was injected for 50 h, during which the properties of water injection were varied. The external mechanical stimuli were varied by applying a stepwise variation in the injection rate, while the external solvent composition was varied by alternately injecting low-salinity

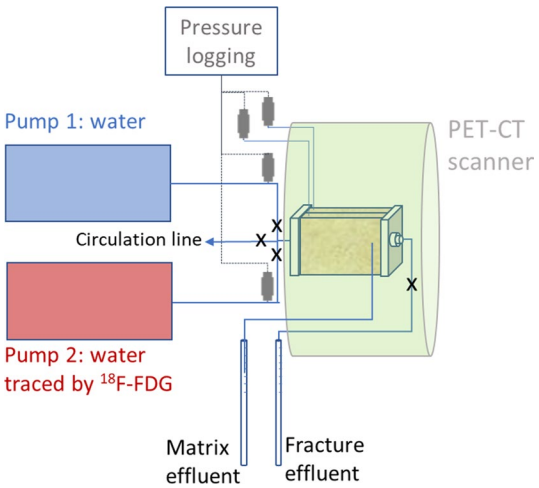

Fig. 3 Schematic of the experimental setup. Flow of water through fracture (gel) and matrix was visualized by PET imaging. Two pumps were used for injection: Pump 1 contained non-labelled water, and Pump 2 contained radiolabelled water. The pumps were connected to a four-way connection close to the core inlet. Each line leading into the connection had manual valves (*X*) that could be opened and closed to separate or connect the desired pump to the core. The third line leading out from the connection was a circulation line: when the salinity of the injected water phase was changed or new ^{18}F-FDG was added, the injected phase was circulated through the connection until the water concentration was stable before injection into the core

and high-salinity water, both variations causing a response in pressure across the gel-filled fracture. Injection rates were varied between (in increasing order) 6–60–120–300 and 499 cm^3/h, and distilled water, with a significantly decreased salinity compared to the gel solvent, constituted the low-salinity water phase in this experiment. PET imaging was applied to determine wormhole development and response to external stimuli. Small volumes of radioactive water were injected at desired times, and the PET signal was acquired and post-processed into three-dimensional images. Radioactive water injections were not predetermined, but initiated based on the developments in continuously monitored injection and matrix pressures. This flexibility enabled visualization of minute changes in dynamic gel behavior.

3 Results and Discussion

Gel behavior, including blocking efficiency and wormhole width, is generally estimated based on core-scale experiments, where pressure drops and flow rates are measured across opaque core plugs. This work used global measurements of pressure and rate, in addition to visualization by PET-CT, to distinguish dynamic wormhole development. The following sections describe waterflooding through the gel-filled fracture during injection of high- and low-salinity water at different injection rates. The images are presented using two views (Fig. 4): a sagittal, fracture-side view (shows the vertically aligned fracture from the side), and a coronal, top-down view of the core (shows the fracture in the middle of the image. Matrix flow is visually distinguishable on each side of the fracture).

3.1 Gel Rupture

Radioactively traced high-salinity water (i.e., no salinity contrast between the injected water and the gel) was first injected into the fracture to rupture the gel in place. A low

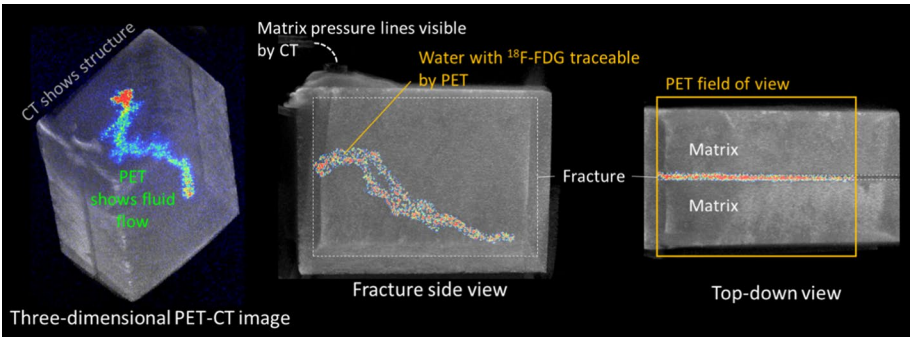

Fig. 4 PET-CT imaging is an efficient tool to determine wormhole behavior. The fracture-side view shows the vertically aligned fracture from the side, to determine the development of wormholes through gel. The top-down view shows the fracture in the middle of the image, and matrix flow can be distinguished on each side of the fracture. The core and fracture localization were determined from CT images (gray scale). The colored signal is radioactive water flowing through the gel-filled fracture, measured by PET. All images were reconstructed in 5-min time intervals. CT was used to localize the PET signal, but PET images were reconstructed without attenuation correction due to beam hardening effects in the CT images

injection rate of 6 ml/h was used. Gel rupture was achieved at a pressure gradient of 5.7 psi/ft, which is in the lower range of previously measured rupture pressures for the same core material, gel placement rate and volume (Brattekås et al. 2015). An increase in injection rate to 60 ml/h led to a brief increase in pressure to 6.7 psi/ft (Fig. 5), as water displaced additional gel around the wormhole. The gel rupture path was measured by PET at $t = 0.35$–0.45 h, when the pressure gradient was stable after gel rupture (Fig. 5). The gel rupture path (here referred to as a "wormhole") was non-uniform within the fracture volume. The original gel formation is a nucleation and growth process, where many little gel nuclei form, grow and eventually link up, i.e., there is naturally some heterogeneity in the gel structure, as it is not formed in a completely homogeneous process. Consequently, the gel dehydration process also inherently contains heterogeneities. Weaker, less-crosslinked parts of the gel structure will be more prone to dehydration. The weaker points in the heterogeneous structure are presumably found to break the gel during gel rupture, forming a non-uniform wormhole. Highly crosslinked pockets of gel that were the origin of a given growth site may be harder to rupture and reside in the wormhole. Figure 5 shows an example of a large gel pocket, visible as a white patch (no radioactive signal) within the wormhole flow path. Natural fluctuations in the PET detector system cause the textured appearance of the wormhole in Fig. 5, and small gel pockets (< 1 mm) could not be quantified by PET in this experiment.

Injected water may follow three physically feasible flow pathways through the core slab after gel rupture: the matrix, the wormhole and/or the concentrated gel. The matrix and gel are porous and permeable structures, with an ability to conduct fluid flow at elevated pressure gradients. Open wormholes, however, constitute the most likely pathway for flow because of their high conductivity. The wormhole flow path is not expected to be constant, but is generally expected to expand during long-term waterfloods. High pressure gradients may erode the gel along the wormhole, while significant throughput of injected water may dissolve (as well as rupture) polymer/crosslinker in the weaker regions of the gel. Such weak points prevail in the region between nucleation points, eventually mobilizing the highly concentrated gel pockets, or enabling particles from such pockets, to break free and move during brine injection. Mobilization of gel particles would most likely occur near the beginning of a wormhole, because of a greater localized throughput of water.

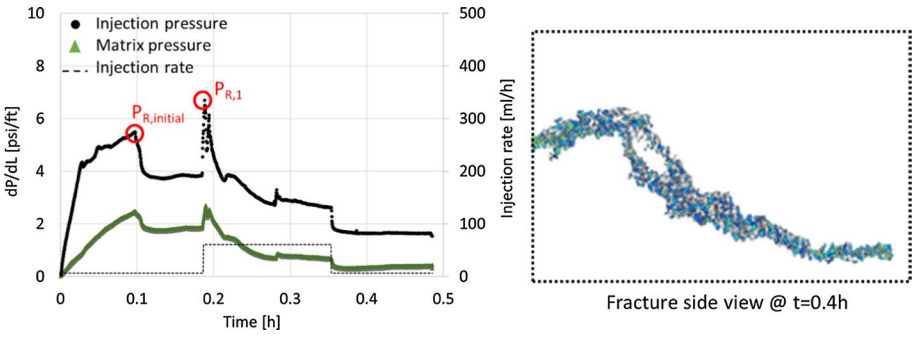

Fig. 5 (Left) pressure development during high-salinity water injection, leading to gel rupture. The development in matrix pressure (green markers) was equal on both sides of the fracture. (Right) Gel rupture path imaged at stable pressure gradients after gel rupture. The PET field of view was shorter than the fracture, and the imaged wormhole therefore stops short of the fracture outlet

3.2 Injection of Low-Salinity Water

The injected water phase was exchanged to low-salinity water at $t \sim 0.5$ h, at stabilized pressure gradients after gel rupture. Contrary to standard waterfloods, reduction in injection brine salinity was shown to improve gel blocking ability over time (Brattekås et al. 2016; Brattekås and Seright 2018). Low-salinity waterflooding continued at a low rate of 6 ml/h between $t = 0.5$–22.8 h. Pressures remained low (< 2 psi/ft) during the first 7 h of injection (Fig. 6). Water flow was imaged in-situ after 1 h of low-salinity water injection (Fig. 6). PET imaging showed that water flow only occurred within a wormhole, which was mostly comparable to the gel rupture path (Fig. 5), with a minor expansion close to the inlet end of the fracture. Erosion and dissolution of the gel in and around the wormhole is expected during long-term water injection. The injection pressure was observed to increase approximately 7 h into the low-salinity water flood, which indicates that the gel blocking efficiency improved. A severely constricted wormhole was imaged at $t \sim 18.9$ h, corresponding to 18.4 h of low-salinity water injection (Fig. 6), and indicates swelling of the fracture-filling gel.

Brattekås et al. (2017) imaged wormhole development during high-salinity waterfloods and found that the wormhole initially occupied 10.8% of the fracture volume and expanded to 34.4% during long-term waterflooding. A quantification of wormhole occupancy within the fracture would be inaccurate in this study, as the PET field of view did not span the entire fracture volume. The relative change in visible voxels (fracture locations containing radioactive water) between time frames can, however, provide a direct measure of wormhole expansion/contraction versus time. ImageJ open source software (https://imagej.net/Downloads) was used for image analysis, and the initial gel rupture path (Fig. 5) constituted the basis for comparison (value = 1). The wormhole expanded with a factor = 1.22 of the initial wormhole within the first hour of low-salinity water injection, but constricted to 0.85 over the next ~ 17.5 h of continued injection. It is evident that wormholes develop differently during low-salinity waterflooding compared to high-salinity waterflooding: A constricted wormhole corroborates the observed increase in pressure during low-salinity

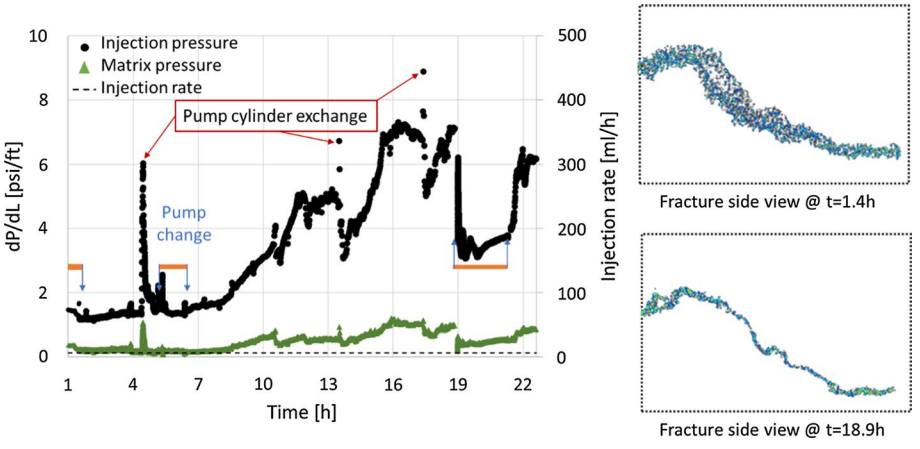

Fig. 6 (Left) pressure development during low-salinity waterflooding, using a low flow rate of 6 ml/h. Radioactive pulse injection is marked by orange color. (Right) PET images of wormhole development during low-rate low-salinity waterflooding. Gel has swelled to constrict the wormhole during 18.4 h of low-salinity waterflooding

injection. Decreasing pressures are commonly observed during high-salinity floods and coincide with decreased gel blocking efficiency due to expanding wormholes.

Swift pressure changes were observed directly following pump changes, due to the opening and closing of valves, or when the two-cylinder pump exchanged cylinders. At elevated pressure gradients, the drop in pressure was more pronounced, for example, when radioactive pulse injection was initiated at $t = 18.9$ h. The constricted wormhole (Fig. 6) was therefore imaged at a decreased pressure gradient compared to non-radioactive water injection. The injection pressure increased by almost 1 psi/ft during radioactive low-salinity injection, and the wormhole development during pressure buildup was captured by PET (Fig. 7). The fracture view suggests that the wormhole spreads within the fracture; however, pressure buildup (left side of Fig. 6) does not support wormhole erosion. Top-down images, showing both the fracture and matrix (Fig. 7), however, offer an explanation: Water is diverted from the fracture and floods into the matrix simultaneously with the dispersion of the wormhole in the fracture. Elevated injection and matrix pressure gradients support water diversion into the matrix. PET imaging shows that water continues to flow through gel, in vicinity of the previously clear wormhole. Gel was previously demonstrated to be permeable, with permeabilities in the micro-Darcy range depending on the gel components and concentrations (Seright 1992). Hence, water may continue to flow through the gel structure at elevated pressure gradients even though gel has swelled sufficiently to constrict the wormhole.

Dispersed wormholes within the fracture during long-term low-salinity water injection were also observed by Brattekås and Seright (2018). The signal-to-noise ratio was, however, low when the observation was made, because radioactive water was continuously injected for several hours (a time frame of several half-lives). Gel may not swell unless the salinity within the gel structure was reduced by diffusion or convection. The dispersion of radioactive signal in the fracture (albeit the long time frame) spurred us to suggest diffusion of radioactive water into the gel matrix as a possible explanation. Although, in theory, diffusion could occur, it is a very slow process. For small molecules (e.g., salt) in a fluid solvent (e.g., water), the diffusion coefficient is $\sim 10^{-5}$ cm^2/s, and diffusion could be estimated to approximately 1 cm/day under normal circumstances. HPAM polymer in water diffuses according to a diffusion coefficient around 10^{-8} cm^2/s without the presence of crosslinker.

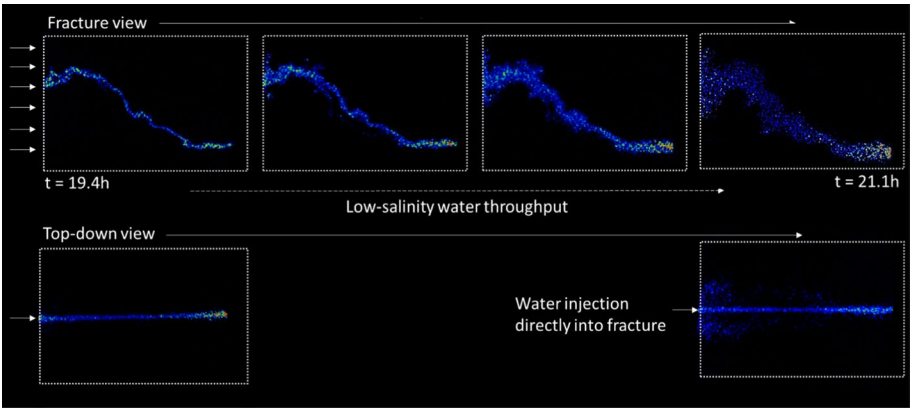

Fig. 7 Wormhole development during continuous low-salinity waterflooding through a gel-filled fracture. Water was injected directly into the vertical fracture

Diffusion would be radically slower (~ 10^{-6} cm/day) in formed polymer gel, and the contribution of diffusion to water spreading and gel swelling in the fracture in the current experiment (short time frames) should therefore be small. Instead, transport of salt may be primarily by forced convection, i.e., flow through the gel enabled by an existing pressure gradient. Even with a gel permeability of 1 micro-Darcy, a pressure gradient of 1 psi/ft would move water by convection at a rate of approximately 1.9×10^{-4} cm/day, which is more than 200 times greater than diffusion in terms of small-molecule movement. Rydzewski (1990) previously attributed bulk gel swelling to osmotic pressure changes caused by the diffusion of sodium chloride between gel and surrounding water. The osmotic pressure difference induced by the salinity contrast between the high-salinity (0.69 M NaCl, 0.23 M $CaCl_2$, and 0.0246 M $MgCl_2$) and low-salinity water (distilled water, 0) used in this study was calculated to be in the order of 500 psi. Osmotic pressure gradients must therefore be considered as a significant contributor to fluid transportation within the gel structure and, consequently, gel re-swelling.

3.3 Second Gel Rupture

The injection pressure fluctuated around the level of initial gel rupture when low-salinity water was injected for more than 15 h (Fig. 8). The water injection rate was increased to 60 ml/h at $t = 22.78$, causing a swift increase in pressure, and a second gel rupture. The new rupture pressure was measured at 15.3 psi/ft—more than twice as high as the initially measure rupture pressure. Gel rupture occurred in a new location, not coinciding with the initial wormhole (Fig. 8). Neither phenomenon was observed or reported during high-salinity waterfloods, where the initial rupture pressure is the highest attainable pressure during subsequent water injection. Brattekås et al. (2017) observed that new rupture paths were added to the existing wormhole when the water injection rate was increased during high-salinity water injections, but did not observe new wormholes forming. Gel rupture location is determined by gel strength and thus directly related to the polymer concentration in the gel. The establishment of a new rupture path indicates that gel has swelled to constrict the original wormhole and that this gel is stronger than the gel present in the remaining fracture volume. This is an interesting observation, considering that the overall polymer concentration in the fracture is static in this experiment. Neither gel nor polymer was added

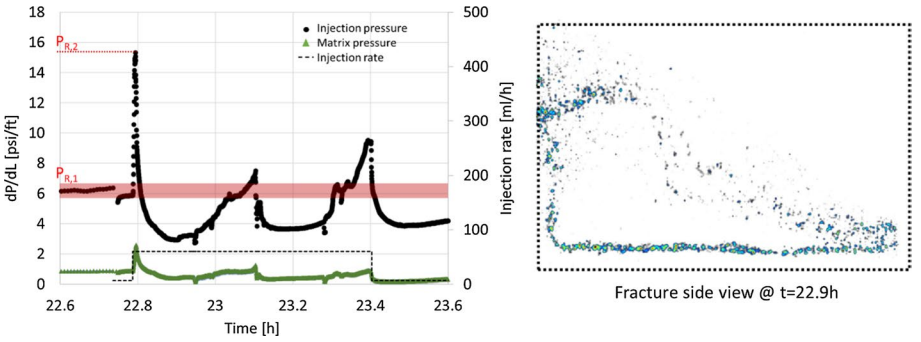

Fig. 8 (Left) pressure development during low-salinity water injection at 60 ml/h. A second, higher, gel rupture pressure was measured. (Right) gel rupture pattern imaged at stable pressure gradients after gel rupture

to the fracture after the initial gel placement, and the only injected fluid was water with a varying salt content. It is possible that the polymer content in the gel decreased during long-term water injection due to gel dissolution, but the effluent was not analyzed to quantify possible chemical content.

Water injection continued at 60 ml/h for 0.6 h, and several consecutive pressure peaks were recorded during this time—all at higher pressure gradients than the initially measured gel rupture pressure. PET imaging showed that all injected water passed through the fracture. Water diversion into the matrix was not detected by PET imaging, and this observation was corroborated by low matrix pressure gradients. The combination of pressure measurements and images indicates that mechanical gel strength increased during low-salinity waterflooding, regardless of possible flush-out of polymer particles from the fracture. Therefore, water passes through the gel-filled fracture at higher pressure gradients than measured during high-salinity water injection.

The injection rate was reduced to 6 ml/h after a third recorded pressure peak, and low-salinity water injection continued. Within a few hours after second gel rupture, the injection pressure again increased above the level of initial gel rupture (Fig. 9). Flow within the fractured system was captured by PET (Fig. 10) from $t=25.5$ to 28.8 h. The injection pressure was below the initial gel rupture pressure at $t=25.5$ h, and in-situ visualization of the injected radioactive water showed that the main flow paths were through clearly distinguishable wormholes in the fracture. Water did not enter the matrix. Within the next 3 h, however, the areal extent of wormholes in the fracture increased and water was simultaneously diverted into the matrix (Fig. 10). The injection pressure increased above the initial gel rupture pressure at $t=28.8$ h—at which time the wormhole appeared widespread in the fracture and matrix flow was evident (Fig. 10). The pressure increase above the level of initial rupture, combined with visual confirmation of water diversion from the fracture, suggests that the gel has once more swelled to constrict the wormholes. Water still transported through the gel at elevated pressure gradients, but the radioactive signal was dispersed, which suggested that water did not flow dominantly through unique wormhole pathways. Gel was previously demonstrated to be porous but have low permeability, which means it can conduct water flow at elevated pressure gradients without having ruptured. The combined observations from Figs. 9 and 10 could indicate a shift in gel behavior: from a fractured to a porous medium. There are no indications (or measurements) to suggest that the permeable gel is uniformly concentrated. One possible explanation for the observed gel behavior may therefore pertain to highly concentrated gel pockets residing in the wormhole. By sufficient swelling of such gel pockets, the wormhole

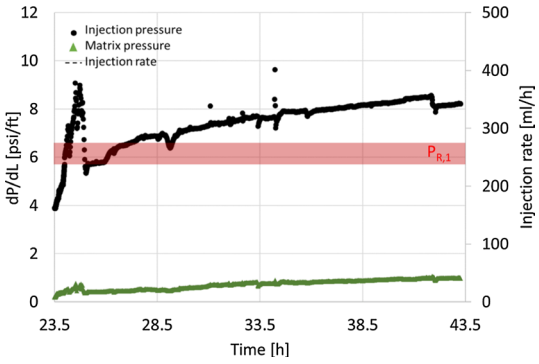

Fig. 9 Pressure development during continuous low-rate, low-salinity water injection. The green markers represent matrix pressure

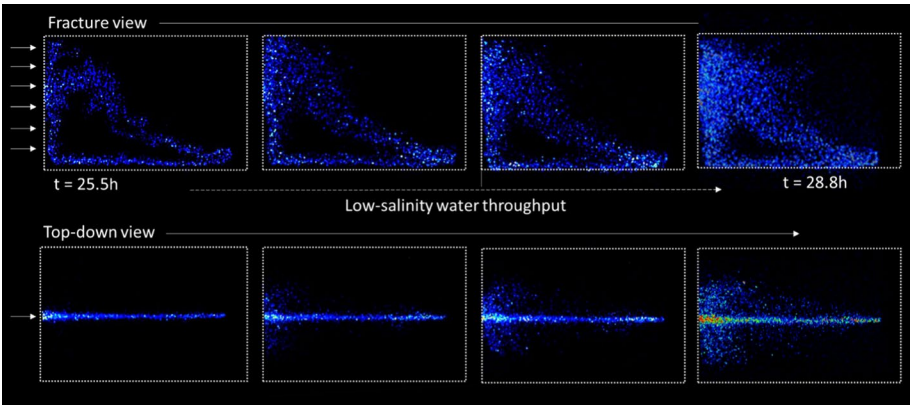

Fig. 10 Flow pattern development as the injection pressure increases during low-rate, low-salinity water injection. At $t = 25.5$ h (left), water flows through clearly distinguishable wormholes in the fracture (fracture-view image) and does not enter the matrix (top-down view). As time passes, and the pressure gradient across the fracture increases, water is diverted into the matrix (visible in the top-down view images). Simultaneously, the gel swells, but continues to transport fluids (visible by fracture view images) as a low-permeability, porous medium

could transform from an open conduit to a porous conduit—consisting of swollen gel islands with interspersed water.

3.4 Third Gel Rupture

The injection pressure continued to increase until $t \sim 44.5$ h, when the injection rate was increased in several consecutive steps (from 6 to 60, 120, 300 ml/h) to impact the pressure gradient and investigate the resulting gel behavior. At the first consecutive rate increase (to 60 ml/h), gel rupture occurred for the third time and was measured at 19.4 psi/ft—more than three times higher than the initially measured gel rupture pressure (Fig. 11). Gel rupture occurred in previously established wormholes: one wormhole spanning diagonally across the fracture (top to bottom), established during initial gel rupture, and another wormhole along the bottom of the fracture, established during second gel rupture. The two wormholes are interconnected at the start of the fracture. New rupture paths were not formed during the third gel rupture, but an increase in wormhole diameter was observed at increased injection rates, due to gel erosion and dissolution. The injection rate was reduced back to 6 ml/h at $t = 45.1$ h, and within 1.5 h, the injection pressure stabilized above the initial gel rupture. Within this time span, PET imaging showed dispersion of radioactive water in the fracture and simultaneous diversion of water into the matrix. Full fracture blocking was achieved within 2.5 h after the third gel rupture. The quick recovery of gel blocking efficiency and the increase in measured rupture pressures strongly implicate a continued increase in gel strength. Strengthening of gel during long-term waterflooding was not previously observed.

3.5 Comparing Water Injection with and Without Salinity Contrast

The injected water composition was exchanged to high-salinity water (composition equal to the gel solvent) at $t = 46.95$ h, causing an immediate decrease in injection

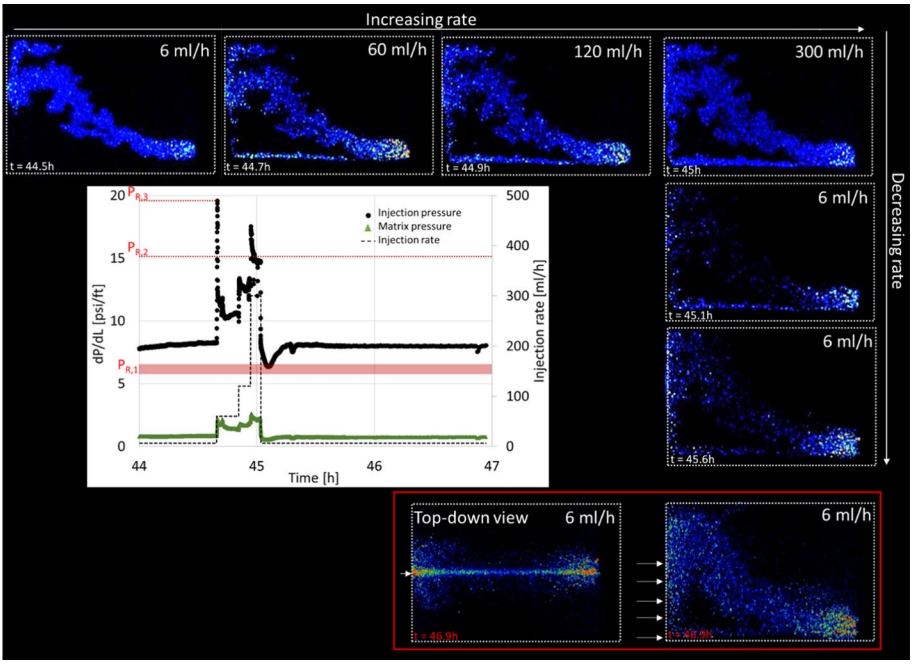

Fig. 11 Pressure development and PET visualization of gel rupture and following full recovery of gel blocking efficiency. New wormholes were not formed during third gel rupture, which occurred in the wormholes established during initial and second rupture. Gel recovery was very quick, and the fracture was fully blocked within 2.5 h after rupture

pressure (Fig. 12). Within 0.2 h of high-salinity water injection, the injection pressure was reduced to, and stabilized at, the same level as attained after gel rupture during initial high-salinity water injection. Diffusion cannot change the salinity of substantial volumes of gel within this time frame, which suggests that some flow occurred through gel (for example, as previously suggested, water flows between swollen pockets of highly concentrated gel residing in the initial wormhole), or that diffusion was relatively fast due to the small size of such gel pockets.

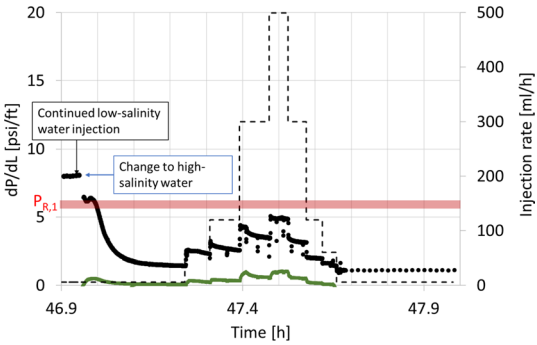

Fig. 12 Pressure development (primary *y*-axis) during high-salinity waterflooding at different injection rates (secondary *y*-axis)

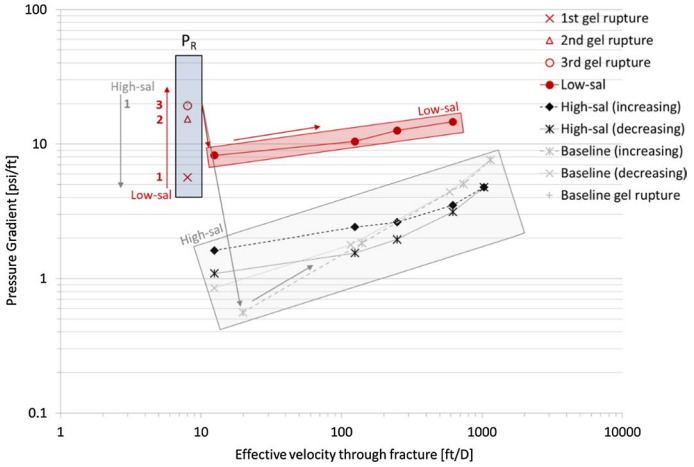

Fig. 13 Pressure gradient measured during waterflooding of ruptured gel (flow through fracture only), using high- and low-salinity water. Previously measured pressures after long-term high-salinity water injection (Brattekås et al. 2015) are also included (denoted "baseline") and are in good agreement with the values achieved after low-salinity waterflooding

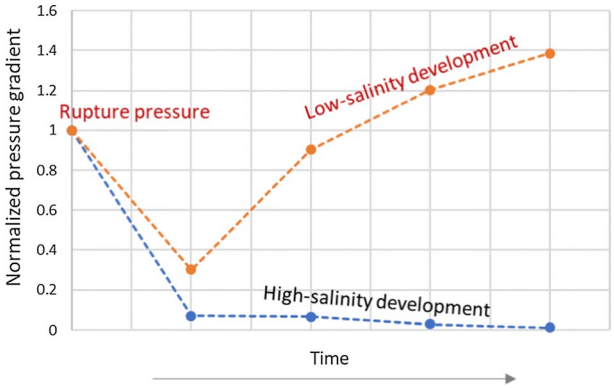

Fig. 14 Development in stable pressure gradients at a flow rate of 6 ml/h normalized to the initial gel rupture pressure. Low-salinity water injection in this work compared to high-salinity water injection from Brattekås et al. (2015)

After stabilization of the pressure gradient, the water injection rate was varied stepwise (increasing from 6 ml/h to 60, 120, 300 and 499 ml/h and then decreasing from 499 ml/h to 300, 120, 60 and 6 ml/h) and stable pressure gradients were measured for each rate and compared to pressure gradients attained during low-salinity water injection, as well as previously published results (Figs. 13, 14). Note that this comparison only considers ruptured gel, i.e., the pressure gradients are measured when water passes through the fracture, without water diversion into the matrix. Pressure gradients achieved during low-salinity injections were clearly higher (factor 5 (minimum) to 7.5 (maximum) higher) than during high-salinity injection, which indicates restriction of fracture flow–presumably caused by gel swelling.

Gel rupture pressure (P_R) development is shown in Fig. 14. During high-salinity waterfloods, the initial rupture pressure was the highest pressure achieved. On the contrary, during low-salinity water injection, the gel shows a unique ability to repair and strengthen itself, and the stabilized pressure gradients during waterfloods through gel

increase above the initial gel rupture pressure. This contradiction, where gel strength improves after rupture, has to our knowledge not previously been observed or reported and indicates that dynamic injection of low-salinity water not only counteracted, but even reversed, mechanical gel degradation.

3.6 Blocking Mechanism Revealed

Gel was previously demonstrated to be porous and of low permeability, while at the same time being elastic. Determining the dynamic behavior of fracture-filling gel during subsequent water injection is therefore a complex problem, which was attempted to be solved in this paper by applying simultaneous pressure measurements and in-situ imaging.

Full gel blocking of a fracture during subsequent fluid injection is generally only achieved when the injection pressure gradient is kept below the gel rupture pressure. If the pressure gradient is increased above this level, gel rupture occurs and fluids predominantly flow through the fracture in very permeable wormholes. PET imaging showed that a non-uniform wormhole formed during gel rupture, which is expected after preformed gel injection, promoting non-uniform gel dehydration by leakoff. After gel rupture, fracture blocking efficiency is expected to decrease, due to erosion and dissolution of the gel around the wormhole. Wormhole formation and development was previously observed during high-salinity water injection using PET imaging, which was compared to current low-salinity injection in the previous sections.

Improved gel blocking efficiency after rupture was observed during low-salinity water injection, both in the current and in previous studies, when the salinity of the injected water was reduced with respect to the gel solvent. In this paper, radioactively labeled water was injected during short time intervals and thereafter flushed out of the fracture, to capture clear images of gel blocking improvement. The main observations were:

- *Gel swelling occurred and constricted the wormholes*. Imaging suggests that gel swells uniformly around the wormholes to constrict them (Fig. 6). Gel particles swelling and clogging the wormholes in given locations were previously suggested as a mechanism for improved gel blocking, but is not indicated in the current work. Clogging of the fracture by mobile, swollen gel particles would most likely occur at narrow constrictions in the wormhole. Imaging showed that water diversion into the matrix consistently started at the inlet end of the core slab, where the wormhole is generally larger due to higher-pressure localized water throughput. Gel particle blocking at narrow constrictions further into the fracture would be implied by water diversion into the matrix starting at the constricted location and a strong fracture signal upstream of said location.
- *Gel continued to transport water*. Water diversion into the matrix was visible by PET imaging and corroborated by increasing matrix pressures. Simultaneously, the injection pressure increased above the level of initial gel rupture, and imaging showed that water was also diverted away from the previously open wormholes and into the fracture-filling gel. Water diversion into gel was evenly distributed throughout the length of the fracture (which also indicates gel swelling rather than wormhole clogging). The passage of water into the fracture-filling gel, rather than out of the fracture, is interesting and supports the previous demonstrations of gel as a permeable and porous medium.

Both observations support that improved blocking occurs because of gel swelling and wormhole constriction; however, two slightly different root causes can be suggested. First, swelling of the gel cake adjacent to the wormhole will constrict the wormhole from the outside. The initial wormhole therefore becomes narrower and finally collapses. Figure 6 suggests this possibility. Second, the existence of individual gel pockets residing in the wormhole promotes improved gel blocking upon swelling, finally restricting fracture flow completely. The quick return to a less-blocking gel during high-salinity flooding supports this possibility. Individual gel islands in the wormhole are quickly contacted by low-salinity water (due to convection rather than diffusion), which promotes quick swelling and de-swelling as occasionally observed in the experiment.

Another important observation was that the rupture pressure increased. All rupture pressures were measured using the same elevated injection rate of 60 cm^3/h and increased from 6.7 to 15.3 psi/ft and finally 19.4 psi/ft. A consecutive increase in rupture pressure with time and water throughput was previously not observed and indicates an increasing gel strength during low-salinity waterflooding.

In previous imaging attempts (Brattekås and Seright 2018), the wormholes gradually became visually indistinct during long-term low-salinity waterflooding and appeared to be widespread in the fracture. Wider wormholes should contribute to a decreasing pressure gradient, yet an increase in pressure was observed, and we concluded: "The calculated average wormhole width from pressure measurements, suggests a decreasing wormhole size to 1% of the original size.[…] The smaller calculated wormhole width indicates that a decreased radioactive signal in the fracture should be expected. It remains unclear whether the indistinct wormholes, visualized by PET, were descriptive of the gel behavior during flooding, and we suspect that diffusion of radioactive water into the gel may have occurred during long-term waterflooding." The current experiment injected low-salinity water over a long time period, but injection of radioactive water was performed over shorter time spans. Dispersed wormholes were also observed in this work and were found to occur simultaneously as water was diverted into the rock matrix. Indistinct wormholes visualized by PET on two occasions are therefore descriptive of water flow through gel after re-swelling.

4 Conclusions

Gel behavior is well mapped during subsequent waterfloods, when the salinity of the injected water matches the gel solvent: The pressure gradient imposed on the gel may increase up to a certain level before the gel ruptures. After gel rupture, water predominantly flows through wormholes and the gel treatment becomes less efficient with time. Improved fracture blocking was not previously reported during high-salinity waterfloods—nor was more than one (initial) gel rupture pressure. Brattekås et al. (2017) observed, using PET-imaging, that increasing water injection rates influenced the geometry of the already established wormhole, but new wormholes were not created. Gel behavior during low-salinity water injection was mapped in this work, providing new observations:

1. A reduction in injected water salinity with respect to the gel solvent improves gel blocking with time and water throughput.
2. PET imaging showed that the main contributor to improved blocking was gel swelling.
3. The wormholes were uniformly constricted along the fracture length, suggesting that gel swelling occurred either: (1) by swelling of the concentrated gel cake enclosing

the wormholes and/or (2) by swelling of individual highly concentrated gel pockets, continuing to reside within the wormhole after rupture.
- Re-swelled gel continued to transport water. Injected water was diverted into the matrix at elevated pressure gradients, but also continued to flow through gel, which indicates that the gel behaves as a porous, low-permeable structure.
- Water transport into gel was necessary to reduce gel salinity and promote gel swelling and was likely achieved by convection due to imposed pressure coupled with high osmotic pressure gradients.
- The gel's ability to swell promoted gel blocking after rupture. Gel blocking improved with time and low-salinity water throughput, without the use of chemicals.
- Three distinct rupture pressures were measured, increasing with time and water throughput, from 6.7 to 19.4 psi/ft in 45 h of low-salinity waterflooding.

Acknowledgements Open Access funding provided by University of Bergen. The imaging was performed at the Molecular Imaging Center at the University of Bergen, Norway. Special thanks to chief scientist Heidi Espedal for help during PET imaging. The custom-made end pieces were made by the mechanical workshop at the Department of Physics and Technology at the University of Bergen, Norway. The authors thank four anonymous reviewers for their contributions to the paper.

References

Aalaie, J., Rahmatpour, A., Vasheghani-Farahani, E.: Rheological and swelling behavior of semi-interpentrating networks of polyacrylamide and scleroglucan. Polym. Adv. Technol. **20**, 1102–1106 (2009)

Al-Sharji, H.H., Grattoni, C.A., Dawe, R.A., Zimmerman, R.W.: Pore-scale study of the flow of oil and water through polymer gels. In: SPE Annual Technical Conference and Exhibition. Houston, TX, Society of Petroleum Engineers (1999)

Andersen, P.Ø., Lohne, A., Stavland, A., Hiorth, A., Brattekås, B.: Core scale modeling of polymer gel dehydration by spontaneous imbibition. SPE J. **24**(03), 1201–1219 (2019)

Bai, B.J., Li, L.X., Liu, Y.Z., Liu, H., Wang, Z.G., You, C.M.: Preformed particle gel for conformance control: factors affecting its properties and applications. SPE Reserv. Eval. Eng. **10**(4), 415–422 (2007)

Brattekås, B., Fernø, M.A.: New insight from visualization of mobility control for enhanced oil recovery using polymer gels and foams. In: Romero-Zèron, L. (ed.) Chemical Enhanced Oil Recovery (cEOR)—A Practical Overview. InTech, Rijeka (2016)

Brattekås, B., Seright, R.S.: Implications for improved polymer gel conformance control during low-salinity chase-floods in fractured carbonates. J. Pet. Sci. Eng. **163**, 661–670 (2018)

Brattekås, B., Haugen, Å., Graue, A., Seright, R.S.: Gel dehydration by spontaneous imbibition of brine from aged polymer gel. SPE J. **19**(01), 122–134 (2014)

Brattekås, B., Pedersen, S.G., Nistov, H.T., Haugen, A., Graue, A., Liang, J.-T., Seright, R.: Washout of Cr(III)-acetate-HPAM gels from fractures: effect of gel state during placement. SPE Prod. Oper. **30**(02), 99–109 (2015)

Brattekås, B., Graue, A., Seright, R.: Low-salinity chase waterfloods improve performance of Cr(III)-acetate hydrolyzed polyacrylamide gel in fractured cores. SPE Reserv. Eval. Eng. **19**(02), 331–339 (2016)

Brattekås, B., Steinsbø, M., Graue, A., Fernø, M.A., Espedal, H., Seright, R.S.: New insight into wormhole formation in polymer gel during water chase floods with positron emission tomography. SPE J. **22**(01), 32–40 (2017)

Brattekås, B., Seright, R., Ersland, G.: Water leakoff during gel placement in fractures: extension to oil-saturated porous media. SPE Prod. Oper. (2019). https://doi.org/10.2118/190256-PA
Degueldre, C., Pleinert, H., Maguire, P., Lehman, E., Missimer, J., Hammer, J., Leenders, K., Bock, H., Townsend, D.: Porosity and pathway determination in crystalline rock by positron emission tomography and neutron radiography. Earth Planet Sci. Lett. **140**(1–4), 213–225 (1996)
Ely, J.W., Herndon, R.A.: Fracturing fluids and additives. In: Miskimins, J. (ed.) Hydraulic Fracturing: Fundamentals and Advancements, pp. 165–191. Society of Petroleum Engineers, Richardson (2019)
Fernø, M.A., Gauteplass, J., Hauge, L.P., Abell, G.E., Adamsen, T.C.H., Graue, A.: Combined positron emission tomography and computed tomography to visualize and quantify fluid flow in sedimentary rocks. Water Resour. Res. **51**, 7811–7819 (2015)
Ganguly, S., Willhite, G.P., Green, D.W., McCool, C.S.: The effect of fluid leakoff on gel placement and gel stability in fractures. SPE J. **7**(03), 309–315 (2002)
Haugan, A.: A low-cost PET system for use in flow experiments of porous media. In: SPE Annual Technical Conference and Exhibition. Dallas, TX (2000)
Hoff, W.D., Wilson, M.A., Benton, D.M., Hawkesworth, M.R., Parker, D.J., Fowles, P.: The use of positron emission tomography to monitor unsaturated water flow within porous construction materials. J. Mater. Sci. Lett. **15**(13), 1101–1104 (1996)
Horkay, F., Tasaki, I., Basser, P.J.: Osmotic swelling of polyacrylate hydrogels in physiological salt solutions. Biomacromol **1**, 84–90 (2000)
ImageJ: free open source software. https://imagej.net/Downloads
Khalili, A., Basu, A.J., Pietrzyk, U.: Flow visualization in porous media via positron emission tomography. Phys. Fluids **10**(4), 1031–1033 (1998)
Krevor, S.C.M., Pini, R., Zuo, L., Benson, S.M.: Relative permeability and trapping of CO_2 and water in sandstone rocks at reservoir conditions. Water Resour. Res. **48**(2), W02532 (2012)
Krishnan, P., Asghari, K., Willhite, G.P., McCool, C.S., Green, D.W., Vossoughi, S.: Dehydration and permeability of gels used in in-situ permeability modification treatments. In: SPE/DOE Improved Oil Recovery Symposium. Society of Petroleum Engineers, Tulsa, OK (2000)
Kulenkampff', J., Gruundig, M., Richter, M., Enzmann, F.: Evaluation of positron-emission-tomography for visualisation of migration processes in geomaterials. Phys. Chem. Earth **33**(14–16), 937–942 (2008)
Liu, J., Seright, R.S.: Rheology of gels used for conformance control in fractures. SPE J. **6**(02), 120–125 (2001)
Maguire, R.P., Missimer, J.H., Emert, F., Townsend, D.W., Dollinger, H., Leenders, K.L.: Positron emission tomography of large rock samples using a multiring PET instrument. IEEE Trans. Nucl. Sci. **44**(1), 26–30 (1997)
Pini, R., Vandehey, N.T., Druhan, J., O'Neil, J.P., Benson, S.M.: Quantifying solute spreading and mixing in reservoir rocks using 3-D PET imaging. J. Fluid Mech. **796**, 558–589 (2016)
Riskedal, H., Tipura, L., Howard, J., Graue, A.: NMR monitoring of spontaneous brine imbibition in carbonates. Society of Core Analysts, Abu Dhabi (2008)
Romero-Zeron, L.B., Hum, F.M., Kantzas, A.: Characterization of crosslinked gel kinetics and gel strength by use of NMR. SPE Reserv. Eval. Eng. **11**(03), 439–453 (2008)
Rydzewski, R.: Swelling and shrinking of a polyelectrolyte gel induced by a salt solution. Contin. Mech. Thermodyn. **2**, 77–97 (1990)
Seright, R.S.: Impact of permeability and lithology on gel performance. In: SPE/DOE Enhanced Oil Recovery Symposium. Society of Petroleum Engineers, Tulsa, OK (1992)
Seright, R.S.: An alternative view of filter-cake formation in fractures inspired by Cr(III)-acetate-HPAM gel extrusion. SPE Prod. Facil. **18**(1), 65–72 (2003a)
Seright, R.S.:Washout of Cr(III)-acetate-HPAM gels from fractures. In: International Symposium on Oilfield Chemistry. Society of Petroleum Engineers, Houston, TX (2003b)
Sydansk, R.D., Romero-Zerôn, L.: Reservoir Confromance Improvement. Society of Petroleum Engineers (SPE), Richardson (2011)
Tie, H.: Oil recovery by spontaneous imbibition and viscous displacement from mixed-wet carbonates. Ph.D. thesis, The University of Wyoming (2006)
Tipura, L.: Wettability characterization by NMR T2 measurements in edwards limestone. Master Thesis, University of Bergen (2008)
Tu, T.N., Wisup, B.: Investigating the effect of polymer gels swelling phenomenon under reservoir conditions on polymer conformance control process. In: International Petroleum Technology Conference. International Petroleum Technology Conference, Bangkok, Thailand (2011)
Willhite, G.P., Pancake, R.E.: Controlling water production using gelled polymer systems. SPE Reserv. Eval. Eng. **11**(3), 454–465 (2008)
Wilton, R., Asghari, K.: Improving gel performance in fractures: chromium pre-flush and overload. J. Can. Pet. Technol. **46**(02), 33–39 (2007)

Zahasky, C., Benson, S.M.: Micro-positron emission tomography for measuring sub-core scale single and multiphase transport parameters in porous media. Adv. Water Resour. **115**, 1–16 (2018)
Zahasky, C., Kurotori, T., Pini, R., Benson, S.M.: Positron emission tomography in water resources and subsurface energy resources engineering research. Adv. Water Resour. **127**, 39–52 (2019)
Zhang, H., Bai, B.: Preformed-particle-gel transport through open fractures and its effect on water flow. SPE J. **16**(2), 388–400 (2011)